JACS
JOURNAL OF THE AMERICAN CHEMICAL SOCIETY
Article
pubs.acs.org/JACS

Building a Multifunctional Aptamer-Based DNA Nanoassembly for Targeted Cancer Therapy

Cuichen Wu,[†,§] Da Han,[†,§] Tao Chen,[†] Lu Peng,[†] Guizhi Zhu,[†] Mingxu You,[†] Liping Qiu,[‡] Kwame Sefah,[†] Xiaobing Zhang,*[,‡] and Weihong Tan*[,†,‡]

[†]Department of Chemistry and Department of Physiology and Functional Genomics, Center for Research at Bio/Nano Interface, Shands Cancer Center, UF Genetics Institute and McKnight Brain Institute, University of Florida, Gainesville, Florida 32611-7200, United States

[‡]Molecular Science and Biomedicine Laboratory, State Key Laboratory of Chemo/Bio-Sensing and Chemometrics, College of Chemistry and Chemical Engineering, College of Biology, Collaborative Innovation Center for Chemistry and Molecular Medicine, Hunan University, Changsha 410082, China

Supporting Information

ABSTRACT: The ability to self-assemble one-dimensional DNA building blocks into two- and three-dimensional nanostructures via DNA/RNA nanotechnology has led to broad applications in bioimaging, basic biological mechanism studies, disease diagnosis, and drug delivery. However, the cellular uptake of most nucleic acid nanostructures is dependent on passive delivery or the enhanced permeability and retention effect, which may not be suitable for certain types of cancers, especially for treatment in vivo. To meet this need, we have constructed a multifunctional aptamer-based DNA nanoassembly (AptNA) for targeted cancer therapy. In particular, we first designed various Y-shaped functional DNA domains through predesigned base pair hybridization, including targeting aptamers, intercalated anticancer drugs, and therapeutic antisense oligonucleotides. Then these functional DNA domains were linked to an X-shaped DNA core connector, termed a building unit, through the complementary sequences in the arms of functional domains and connector. Finally, hundreds (~100−200) of these basic building units with 5′-modification of acrydite groups were further photo-cross-linked into a multifunctional and programmable aptamer-based nanoassembly structure able to take advantage of facile modular design and assembly, high programmability, excellent biostability and biocompatibility, as well as selective recognition and transportation. With these properties, AptNAs were demonstrated to have specific cytotoxic effect against leukemia cells. Moreover, the incorporation of therapeutic antisense oligonucleotides resulted in the inhibition of P-gp expression (a drug efflux pump to increase excretion of anticancer drugs) as well as a decrease in drug resistance. Therefore, these multifunctional and programmable aptamer-based DNA nanoassemblies show promise as candidates for targeted drug delivery and cancer therapy.

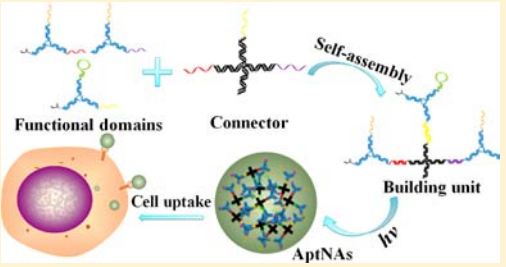

INTRODUCTION

Although nanoparticle- and polymeric-nanomaterial-based therapeutic strategies have been widely introduced into drug delivery and cancer theranostics, challenges still remain in their efficacy and complexity, as well as their biocompatibility.[1,2] To develop a new generation of drug delivery platforms, the emergence of DNA/RNA nanotechnology has allowed the elegant self-assembly of one-dimensional nucleic acid molecules into two- and three-dimensional nanostructures through specific molecular recognition and programmable molecular design, such as hydrogen bonding and π-stacking.[3−17] These 3D nucleic acid nanostructures, which self-assemble by predictable and programmable nucleic acid molecules containing different functional moieties, have attracted increasing attention in the fields of biosensing and disease diagnosis,[18−23] especially as a potential cellular carrier for drug delivery and disease treatment.[24−31] For example, a self-assembled short interference RNA (siRNA) microsponge was produced via a rolling circle transcription to achieve high loading capacity and delivery efficiency for targeted gene silencing in vivo.[32,33] Well-defined, uniformly sized tetrahedral DNA nanoparticles functionalized with siRNA or immunostimulatory CpG oligonucleotides exhibited excellent intracellular biostability and biocompatibility, thus facilitating the efficacy of gene therapy and immunoregulation.[34,35] In addition, self-assembled DNA tubular and triangular origami nanostructures loaded with the anticancer drug doxorubicin circumvented the drug resistance of cancer cells by the inhibition of lysosomal acidification.[36] In contrast to 1D DNA/RNA molecules, the power of self-assembled 3D nucleic acid nanostructures lies in their excellent biostability, high drug payloads, and passive delivery into living cells, even tumors.[37,38]

However, self-assembled nucleic acid nanostructures pose challenges that remain to be solved. First, most 3D nucleic acid nanostructures enter cancer cells or tumors via passive delivery.

Received: September 17, 2013
Published: November 18, 2013

   dx.doi.org/10.1021/ja4094617 | J. Am. Chem. Soc. 2013, 135, 18644−18650

While such passive delivery is satisfactory for prostate or breast cancers with leaky vasculatures,[24,33,34] it may not be suitable for other types of cancers, such as leukemia and lymphoma, thereby impeding broad application in vivo.[32] For active targeting of leukemia, specific recognition ligands aimed at cell receptors or cancer biomarkers are prerequisite for providing enhanced, selective diagnosis and treatment.[35] Second, the complicated modification of tumor targeting ligands, including antibodies or small molecules, into 3D nucleic acid nanostructures has been reported. The difficulties in precisely and programmably controlling functional ligands in 3D nucleic acid nanostructures for clinical trials have not yet been fully explored. Therefore, a facile approach for conjugation of targeting ligands into nucleic acid nanostructures in a controlled manner is still in demand. Third, the disassembly of Watson−Crick base pairings in nucleic acid nanostructures during cellular delivery results from the alternation of nanostructure with in vivo environment.[25] Maintaining biostability of nucleic acid nanoassemblies is a prerequisite for cellular drug delivery. More importantly, instead of having a single functionality on each self-assembled nanostructure, the ability to construct a multifunctional nucleic acid complex capable of active recognition, efficient transportation, and elevated therapeutics would be highly desirable. Through complementary strategies, multifunctional and programmable nucleic acid nanostructures will provide efficient and reliable point-of-care platforms for rapid disease diagnosis, targeted drug delivery, and cancer therapy.

Using a bottom-up modular approach, we report the construction of a multifunctional and programmable aptamer-based DNA nanoassembly (AptNA) to address these challenges. As shown in Figure 1, multifunctional DNA sequences, including aptamer, acrydite-modified single-stranded DNA, and antisense oligonucleotide, are self-assembled to form Y-shaped functional domains, which are then linked to X-shaped connectors to create building units. Different functional elements can be incorporated into the domains of each building unit, including antisense oligonucleotides capable of suppressing the expression of specific cellular proteins,[39] chemical anticancer drugs intercalated in specific DNA base pairs,[40,41] and aptamers, consisting of single-stranded DNAs derived from cell-based systematic evolution of ligands by exponential enrichment (SELEX) for specific recognition of certain cancer cells.[42] By integrating all functional domains into one nanoassembly system, the aptamer moieties can act as a guidance system to target specific cancer cells. Hundreds of these basic building units are then photo-cross-linked into multifunctional and programmable nanoassembly structures with controllable diameters.[24,43,44] The bulky nanoassembly provides many sites available for high-capacity loading of therapeutics or bioimaging agents. In addition, AptNAs show excellent biostability in the physiological environment (pH 7.4), thus avoiding unnecessary leaking of intercalated drugs during delivery.

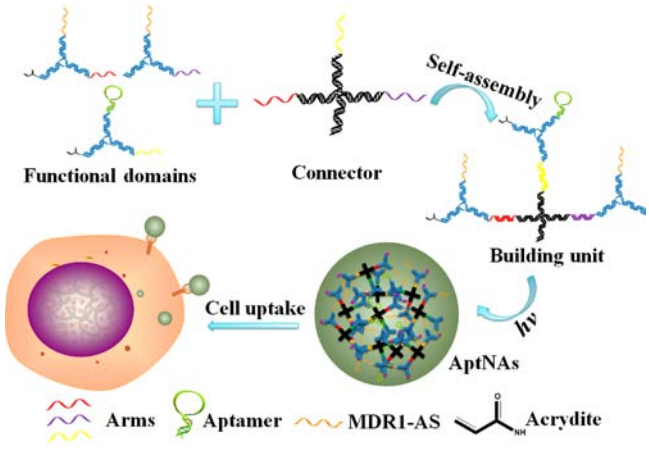

Figure 1. Schematic illustration of the multifunctional self-assembled nanoassembly building units and photo-cross-linked nanoassembly structure. Multifunctional DNA sequences, including aptamers, acrydite-modified single-stranded DNA, and antisense oligonucleotides are self-assembled to form Y-shaped functional domains, which further link via X-shaped connectors to form building units through the complementary arm sequences. Hundreds of these basic building units are then photo-cross-linked into a multifunctional and programmable nanoassembly structure.

RESULTS AND DISCUSSION

Bottom-up Construction of Aptamer-Based DNA Nanoassembly. The working principle of our multifunctional and programmable nanoassembly structure, as shown in Figure 1, is explained in more detail as follows. First, four single-stranded DNAs were self-assembled to form an X-shaped core *connector* via predesigned base-pair hybridization (see Table 1 in the Supporting Information). Each connector had three distinct toehold sequences, called *arms*, at the ends of different branches. To achieve multiple functionalities, Y-shaped DNA functional *domains* with arms complementary to those of the connectors were designed to link with the core connector to form a *building unit*. Various functional groups, for example, targeting aptamers, intercalated anticancer drugs, and therapeutic antisense oligonucleotides, were incorporated in different domains. Thus, each nanoassembly building unit consists of one core connector and three functional domains. Acrydite groups were included in two of the functional domains of each building unit based on the 5′-modification of the oligonucleotides during DNA synthesis. Consequently, the acrydite-modified building units can be further photo-cross-linked to form different nanostructures with controllable diameters.[24,44] Because of the precise design of arm sequences in each building unit, an accurate ratio between different functional moieties (aptamers or antisense oligonucleotides), as well as programmable self-assembled functional domains, can be achieved in the entire nanoassembly.

To demonstrate the precise self-assembly of this modular approach, polyacrylamide gel electrophoresis was used to examine the formation of a single building unit. The smaller mobility of functional domains was observed relative to that consisting of ssDNA (Figure S1a). Mixed in equimolar amounts, all three functional domains were anisotropically and simultaneously linked to the connector with the aid of predesigned arm sequences (Figure S1b, c). Compared to any one of its constituent domains, the self-assembled building unit had less mobility as a result of its collective increased molecular weight. However, the application of photopolymerization changed the geometry and size of these building units to create nanoassemblies composed of many hundreds of building units. Specifically, dynamic light scattering (DLS) revealed that the building units with photoresponsive acrydites formed nanostructures with an initial hydrodynamic diameter of 17 nm, but further increasing to 218 nm after photoillumination for 10 min (Figure S2). Because of the highly efficient photo-

dx.doi.org/10.1021/ja4094617 | J. Am. Chem. Soc. 2013, 135, 18644−18650

polymerization, no peak corresponding to a single building unit was observed in the DLS results, and nanoassemblies displayed spherical structures, as confirmed by transmission electron microscopy (TEM, Figure 2a), such that the diameter of the

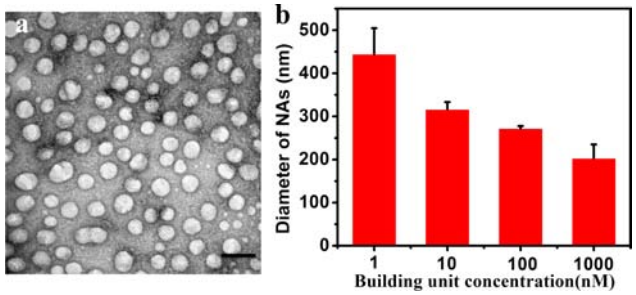

Figure 2. Characterization of aptamer-based DNA nanoassembly structures. (a) TEM image of spherical photo-cross-linked nanostructures. Scale bar: 200 nm. (b) Size-dependent (in diameter) distribution of nanoassemblies based on controllable concentration of building unit.

spherical nanoassembly could be controlled by simply changing the concentration of the building units (Figure 2b). For example, a higher concentration of building units will induce a smaller overall nanostructure diameter because of an elevated ratio of polymeric units over photoinitiators. To more perfectly control the number of building units in each nanoassembly, an alternative cross-linking approach, dendrimerization, can be also employed to form size and shape controllable DNA nanostructures. Thus, this modular, photopolymerization approach can be used to generate size-controllable nanoassembly structures.

Selective Recognition of Target Cancer Cells by AptNAs. The aptamer targeting domains enable the nanoassembly to specifically recognize target cancer cells. As a proof of concept, sgc8 aptamer, which targets CCRF-CEM (T cell acute lymphoblastic leukemia cell line) cancer cells, but not Ramos (B cell human Burkitt's lymphoma), was conjugated into one functional domain of each building unit. After photo-cross-linking, the selective binding affinity of the sgc8-NAs was verified by flow cytometry, which showed a 100-fold fluorescence signal shift over library DNA-NAs for CEM cells (Figure 3a), while no significant shift was observed for Ramos cells treated with sgc8-NAs and library DNA-NAs (Figure 3b). As a result of the multiple building units in the nanoassembly

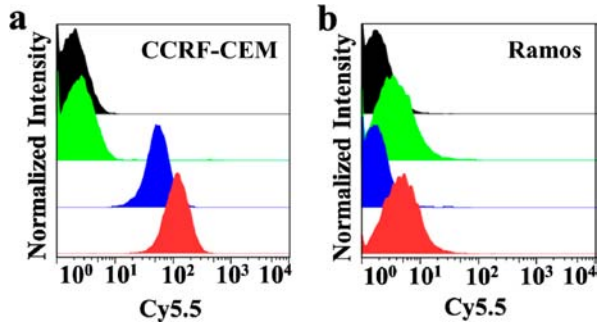

Figure 3. Specific cancer cell recognition via sgc8-NAs. Analytical flow cytometry shows the selective binding of sgc8-modified nanoassemblies to target CCRF-CEM cells (a), but not nontarget Ramos cells (b). Black peak, cells only; green peak, library DNA-NAs; blue peak, sgc8 aptamer only; red peak, sgc8-NAs.

structures, the sgc8-NAs showed an amplified fluorescence signal intensity compared to a single sgc8 aptamer because of signal amplification from multiple signal molecules in each sgc8-NAs. The generality of aptamer-based nanoassemblies was verified using a different aptamer, KK1B10, which can specifically recognize Dox-resistant leukemia cells (K562/D), but not control Ramos cells (Figure S3).[45]

The cellular trafficking of DNA-assembled nanoparticles has been reported by labeling with quantum dots or organic dyes.[24,36] In this study, a DNA intercalated dye, SYBR Green, was used to stain sgc8-NAs to investigate their specific transport into target cancer cells. A strong green fluorescence signal was observed by confocal laser scanning microscopy (CLSM) after incubating sgc8-NAs with CEM cells at 37 °C for 2 h (Figure 4a). However, a slightly green fluorescence signal

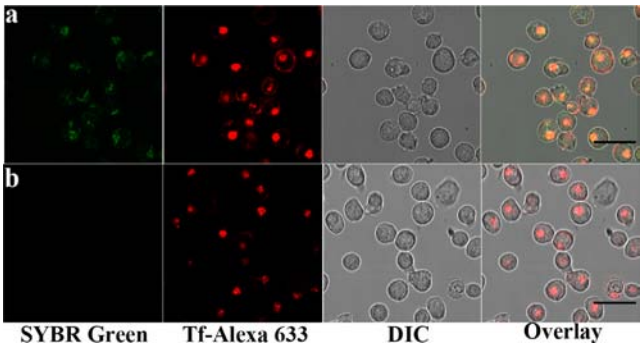

Figure 4. Confocal laser scanning microscopy images of the colocalization of SYBR-Green-stained sgc8-NAs and Tf-Alexa 633 (endosome marker), indicating the specific internalization of sgc8-NAs into CEM cells (a) rather than Ramos cells (b). Scale bar: 20 μm.

was also observed for Ramos cells, possibly because of the nonspecific internalization of nanoassemblies or the leakage of dyes into nontarget cells (Figure 4b). Previous work suggested that the sgc8 aptamer specifically enters CEM cells through receptor-mediated endocytosis; therefore, a colocalization assay was used to demonstrate the final destination of sgc8-NAs in living CEM cells. Most green fluorescence signals from SYBR-Green-intercalated nanoassemblies were overlapped with the red fluorescence generated by transferrin Alexa-633 (a marker for endosomes),[46] which was not seen for Ramos cells. Thus, this aptamer-based nanoassembly has properties of a large nanostructure, including selective targeting and internalization, making it a potential platform for targeted cancer therapy.

Selective Cytotoxicity of Anticancer Drug-Loaded AptNAs. As a consequence of the large number of packed hybridized DNA base pairs, this DNA-assembled nanostructure is spatially well equipped for cargo loading, especially for chemical anticancer drugs such as doxorubicin (Dox) which can preferentially intercalate into double-stranded GC base pairs.[41] Comparing the molecular weight of a single nanoassembly structure to that of a single building unit, it was determined each AptNA contained 100−200 building units, and each building unit was able to provide more than 220 Dox loading sites. Dox fluorescence after intercalation into sgc8-NAs was dramatically quenched with a molar ratio of 1000/1, indicating a high loading capacity of 10 nM sgc-NAs with ~10 μM Dox. We next evaluated the release kinetics of Dox loaded in sgc8-NAs by using a drug diffusion method with MINI Dialysis Units. The sgc8-NAs (50 nM) with a drug payload of 50 μM displayed less than 7% cumulative release in a physiological

dx.doi.org/10.1021/ja4094617 | J. Am. Chem. Soc. 2013, 135, 18644−18650

environment (pH 7.4) in contrast to rapid diffusion in acidic solution (50−60% release) probably due to the influence of the low pH on DNA base pair hybridization and charge effect to Dox-DNA interaction (Figure S4). Thus, Sgc8-NAs exhibited excellent stability with high drug payload under physiological conditions, thus effectively preventing drug leaking while, at the same time, facilitating drug release in an endosome-like environment.

To investigate selective anticancer drug transport into target cancer cells, the uptake of Dox-loaded sgc8-NAs and distribution of intercalated drugs were studied with CEM and Ramos cells using free Dox as a control. For free Dox, confocal imaging results show that a strong fluorescence signal was produced in both CEM and Ramos cells (Figure 5a, b). In contrast, the Dox fluorescence was restored by release from sgc8-NAs in CEM cells, but not Ramos cells, indicating the selective delivery of Dox via the aptamer-based nanoassembly structures (Figure 5c, d). Since it has been demonstrated that Dox offloading from internalized sgc8-NAs is influenced by intracellular location and the corresponding pH environment, we believe that the transported sgc8-NAs-Dox complex first enters cells via endocytosis, followed by residence in endosomes, which then, by their acidic environment, facilitate the rapid release of loaded anticancer drugs, with Dox finally escaping from the endosomes and further widening its distribution in the cytoplasm, and even nucleus. The in vitro cytotoxicity of Dox-loaded sgc8-NAs and free Dox was evaluated by the 3-(4,5-dimethylthiazol-2-yl)-5-(3-carboxymethoxyphenyl)-2-(4-sulfophenyl)-2*H*-tetrazolium (MTS) assay. Free Dox presented dose-dependent cytotoxicity behavior in both CEM and Ramos cells (Figure S5); however, Dox-loaded sgc8-NAs induced an efficient and dose-dependent cytotoxicity only in targeted CEM cells, but not nontarget Ramos cells (Figure 6). Regarding the different dose dependent response of cancer cells to Dox, the largest cytotoxic enhancement was evaluated to be ~3.8-fold with a payload of 0.5 μM Dox in sgc8-NAs for CEM cells (Figure S5). In addition, sgc8-NAs without Dox exhibited negligible cytotoxicity and more than 90% cell viability, even in a 1 μM concentration of building units (Figure S6). These results all indicate that this aptamer-based DNA nanoassembly system possesses potential cancer therapeutic properties, including excellent biocompatibility and highly selective killing efficacy to target cancer cells.

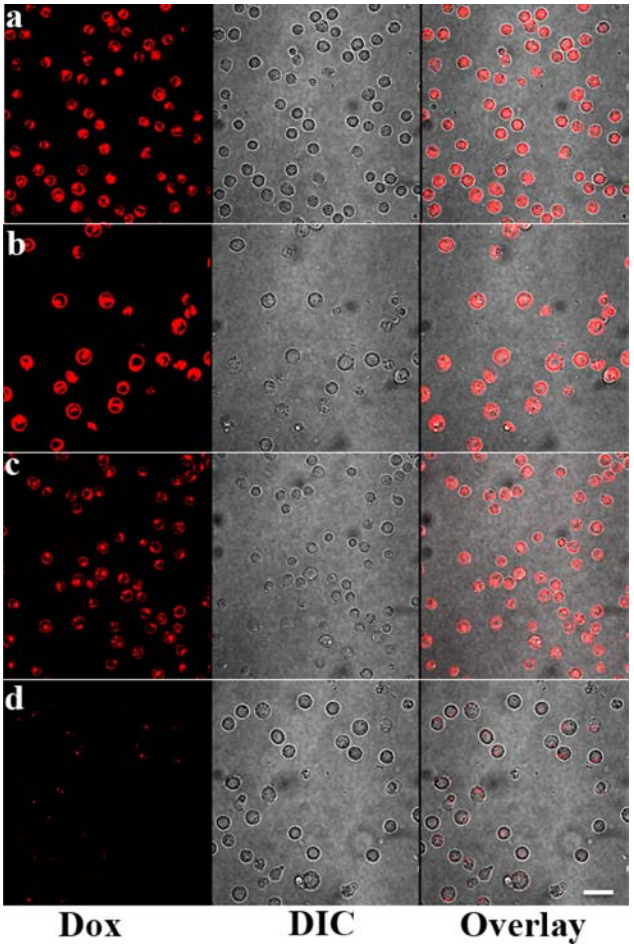

Figure 5. Selective cytotoxicity of Dox-loaded sgc8-NAs against targeted cancer cells. (a−d) Confocal fluorescence imaging shows Dox transport via Dox-loaded sgc8-NAs relative to the same concentration of free Dox to target CEM (a and c) and nontarget Ramos cells (b and d). CEM and Ramos cells were treated with free Dox (a and b) and sgc8-NAs Dox complex (c and d). Scale bar: 20 μm.

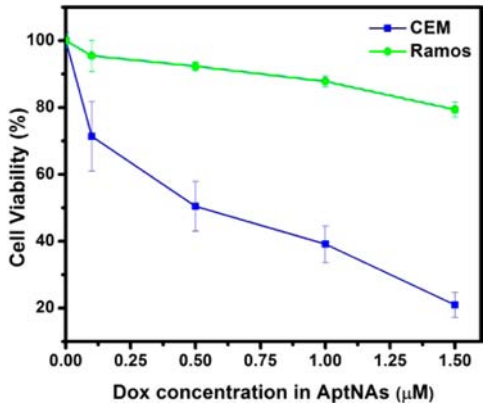

Figure 6. MTS assay was performed to assess the selective cytotoxicity of CEM and Ramos cells treated with sgc8-NA complexes.

Recovery of Anticancer Drug Sensitivity in Drug-Resistant Cancer Cells. Having established the drug loading capability of AptNAs for targeted cancer therapy, the functionalization of therapeutic antisense (AS) oligonucleotides was explored to overcome the obstacle of multidrug resistance (MDR) in chemotherapy. As a proof of concept, a Dox-loaded and MDR1-AS-incorporated KK1B10 aptamer-modified nanoassembly structure was constructed to selectively kill drug-resistant myelogenous leukemia, K562/D.[47,48] MDR1 antisense oligonucleotides have been reported to specifically inhibit the overexpression of P-glycoprotein (P-gp), a membrane glycoprotein which acts as a drug efflux pump to increase excretion of structurally related drugs from cells and to reduce intracellular drug accumulation.[36,49,50] Particularly, the MDR1-AS/KK1B10/NAs-Dox complex was cross-linked with building units consisting of one KK1B10 aptamer and two MDR-AS domains; thus, each nanoassembly had a highly localized concentration of antisense oligonucleotides (~400). After specific recognition and uptake by target drug-resistant K562 cells, the recovery of Dox sensitivity to K562/D was verified by MTS assay. MDR1-AS/KK1B10/NAs-Dox nanostructures showed dose-dependent cytotoxicity and 34% cell viability at 20 μM Dox payload in K562/D cells (Figure 7), in

dx.doi.org/10.1021/ja4094617 | J. Am. Chem. Soc. 2013, 135, 18644−18650

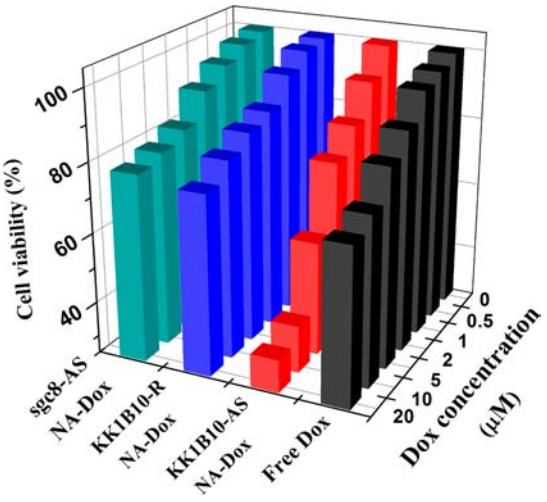

Figure 7. Selective cytotoxicity of drug-resistant K562 cells treated with free Dox, KK1B10-AS NA-Dox, KK1B10-R NA-Dox, and sgc8-AS NA-Dox.

contrast to ~70% metabolically active K562/D cells using 20 μM free Dox, suggesting that the antisense oligonucleotides transported by KK1B10-NAs played a role in inhibiting P-gp expression and decreasing drug resistance. Neither KK1B10 NAs-Dox modified with random oligonucleotides nor sgc8-NA Dox complexes modified with MDR1 AS led to substantial inactivity of K562/D cells, even with a 20 μM Dox payload (76% and 78%), indicating that the selective killing of drug-resistant cancer cells was induced only by KK1B10 NAs-Dox nanostructures modified with MDR1-AS. The viability of K562/D cells initiated a rapid decrease after treatment with either 5 μM free Dox or MDR-AS KK1B10 NAs-Dox complex, essentially because K562/D cells were induced and cultured with a high concentration of Dox (3 μM). The KK1B10 NAs-Dox complexes modified with MDR1-AS provided high drug payload capacity and the synergistic effects of combined chemotherapy and gene therapy for target drug-resistant cancer cells.

CONCLUSION

Based on a modular and photo-cross-linking strategy, we have molecularly constructed a multifunctional and programmable aptamer nanoassembly that can be utilized for the specific recognition and selective cytotoxicity of target cancer cells, as well as act as a drug carrier. This aptamer-based nanoassembly platform exhibits several remarkable features: (1) *Easy modular design, facile assembly and preparation*. All the nanoassemblies mentioned in this study are first self-assembled with basic building blocks in a modular manner, followed by further photopolymerization to form size-controllable nanostructures. (2) *Integrated multifunctionality*. Different functional domains, including targeting aptamers, intercalated anticancer drugs, and therapeutic antisense oligonucleotides, enable this nanoassembly to act as a potential platform for targeted cancer therapy. (3) *High programmability*. The basic building unit provides precise control of the ratio of functional moieties, as well as programmable assembly of functional domains based on the therapeutic purpose. The hybridized double-stranded DNA configuration also allows for thousand-fold loading of anticancer drugs or bioimaging agents in a single nanoassembly. (4) *Good biostability*. Nanoassemblies exhibit enzymatic resistance (Figure S7) and loading stability under physiological conditions. (5) *Excellent biocompatibility*. The nanoassemblies themselves show negligible cytotoxicity, while demonstrating targeted cytotoxicity when modified with the appropriate aptamers. Thus, our multifunctional aptamer-based nanoassemblies will find potential applications for point-of-care diagnosis, efficient drug transportation, and improved targeted cancer therapeutics.

EXPERIMENTAL SECTION

DNA Synthesis. All oligonucleotides were synthesized based on solid-phase phosphoramidite chemistry at a 1 μmol scale using the ABI3400 DNA/RNA synthesizer (Applied Biosystems, Foster City, CA). Acrydite was directly coupled at the 5′-end of oligonucleotides with an extended coupling time. A ProStar HPLC (Varian, Walnut Creek, CA) instrument with a C18 column (Econosil, 5, 250 mm) from Alltech (Deerfield, IL) was used to purify all fabricated DNA. The collected sequences were vacuum-dried and quantified using a Cary Bio-300 UV spectrometer (Varian, Walnut Creek, CA).

Preparation of Building Units and Nanoassembly Structures. Each basic building unit was prepared by incubating equimolar amounts of connector, functional domain 1, functional domain 2, and functional domain 3 at 30 °C for 1 h (10 mM Tris buffer, 15 mM $MgCl_2$, pH 8). The aptamer-based nanoassembly was photopolymerized in aqueous solution containing 0.5% MW Ciba IRGACURE 2959 Photoinitiator Edition 2.4.98 using a portable UV lamp (350 nm) for 10 min.

Cell Culture. CCRF-CEM (human acute lymphoblastic leukemia), Ramos (human Burkitt's lymphoma), and K562 (chronic myelogenous leukemia) cell lines were purchased from ATCC (Manassas, VA). The doxorubicin-resistant K562 cell line (K562/D) was induced and cultured by our lab. All cells were cultured in RPMI 1640 medium (ATCC, Manassas, VA) supplemented with 10% FBS and 100 IU/mL penicillin-streptomycin (Cellgro, Manassas, VA).

Calculation of Building Unit Number. Polymerized NAs were washed and concentrated using an AmiconUltra-0.5 (50K MWKO) concentrator (Millipore, Billerica, MA). The molecular weight of single nanoassembly was measured by a ZetaPALS DLS detector (Brookhaven Instruments, Holtsville, NY) at 25 °C, $(2.4 \pm 0.8) \times 10^7$ g/mol. The molar mass of each building unit was calculated including the modified chemical group, 1.7×10^5 g/mol. The ratio between the molecular weight of single nanoassembly and building unit was the estimated number of building units in polymerized NAs, ~150 ± 50.

Binding Affinity Analysis. CCRF-CEM, Ramos, and K562/D cells were grown at a concentration of 2×10^6 mL^{-1} before the experiments were conducted. Cells (10^6 mL^{-1}) were first washed with washing buffer (500 μL) at 4 °C, followed by staining on ice with different nanoassemblies in binding buffer (200 μL) containing 10% FBS for 20 min. Then, cells were washed with washing buffer (500 μL) three times and incubated with streptavidin PE-Cy5.5 dye solution (100 μL) for another 20 min. Finally, washed cells were suspended in 200 μL of binding buffer for fluorescence detection on a FACScan cytometer (Becton Dickinson Immunocytometry System, San Jose, CA). The fluorescence was determined by counting 10 000 events, and data were analyzed with Flowjo software.

Confocal Fluorescence Microscopy Imaging. All cellular fluorescent images were collected on a FV500-IX81 confocal microscope (Olympus America Inc., Melville, NY) with a 40× oil immersion objective (NA = 1.40, Olympus, Melville, NY). Excitation wavelength and emission filters: Dox, 488 nm laser line excitation, emission BP (580 ± 20) nm filter; Transferrin-Alexa 633, 633 nm laser line excitation, emission BP (670 ± 20) nm filter. Cells (10^6 mL^{-1}) were incubated at 37 °C with Dox or Dox-loaded nanoassembly for 2 h, followed by washing with washing buffer (1 mL) twice and suspension in binding buffer (200 μL) before imaging. Each experiment was analyzed with Fluoview software.

Cytotoxicity Assay. The cytotoxicity of nanoassemblies or Dox-loaded nanoassemblies for each individual type of cell was determined by MTS assay using a CellTiter 96 cell proliferation assay (Promega,

dx.doi.org/10.1021/ja4094617 | J. Am. Chem. Soc. 2013, 135, 18644−18650

Madison, WI). After seeding in 96-well plates and culturing overnight, the cells were incubated with nanoassemblies or Dox-loaded nanoassemblies for 2 h, washed with PBS, and then cultured with fresh medium for future cell growth (48 h). After removing the cell medium, CellTiter reagent (20 μL) diluted in fresh medium (100 μL) was added to each well and incubated for 1−2 h. The absorbance (490 nm) was recorded by using a plate reader (Tecan Safire microplate reader, AG, Switzerland).

■ ASSOCIATED CONTENT

Supporting Information

Synthesized DNA sequences in this work, synthesis of acrydite phosphoramidite, gel electrophoresis image of building unit and connector, DLS measurement, enzymatic resistance of AptNAs, cumulative release evaluation of Dox-loaded AptNAs, cytotoxicity of free Dox to CEM and Ramos, and sgc8-NAs. This material is available free of charge via the Internet at http://pubs.acs.org.

■ AUTHOR INFORMATION

Corresponding Authors

tan@chem.ufl.edu
xbzhang@hnu.edu.cn

Author Contributions

[§]C.W. and D.H. contributed equally to the work.

Notes

The authors declare no competing financial interest.

■ ACKNOWLEDGMENTS

The authors thank Dr. Chaoyong James Yang for constructive suggestions and Dr. K. R. Williams for manuscript review. D.H. acknowledges the ACS Division of Analytical Chemistry Fellowship sponsored by the Society for Analytical Chemists of Pittsburgh. This work is supported by grants awarded by the National Institutes of Health (GM079359 and CA133086). This work is also supported by grants awarded by the National Key Scientific Program of China (2011CB911000 and 2013CB933701), the Foundation for Innovative Research Groups of NSFC (Grant 21221003), and China National Instrumentation Program 2011YQ03012412.

■ REFERENCES

(1) Peer, D.; Karp, J. M.; Hong, S.; Farokhzad, O. C.; Margalit, R.; Langer, R. *Nat. Nano* **2007**, *2*, 751.
(2) Petros, R. A.; DeSimone, J. M. *Nat. Rev. Drug Discovery* **2010**, *9*, 615.
(3) Li, Y.; Tseng, Y. D.; Kwon, S. Y.; d'Espaux, L.; Bunch, J. S.; McEuen, P. L.; Luo, D. *Nat. Mater.* **2004**, *3*, 38.
(4) Goodman, R. P.; Schaap, I. A. T.; Tardin, C. F.; Erben, C. M.; Berry, R. M.; Schmidt, C. F.; Turberfield, A. J. *Science* **2005**, *310*, 1661.
(5) Aldaye, F. A.; Palmer, A. L.; Sleiman, H. F. *Science* **2008**, *321*, 1795.
(6) Yin, P.; Hariadi, R. F.; Sahu, S.; Choi, H. M. T.; Park, S. H.; LaBean, T. H.; Reif, J. H. *Science* **2008**, *321*, 824.
(7) Wang, H.; Yang, R.; Yang, L.; Tan, W. *ACS Nano* **2009**, *3*, 2451.
(8) Afonin, K. A.; Bindewald, E.; Yaghoubian, A. J.; Voss, N.; Jacovetty, E.; Shapiro, B. A.; Jaeger, L. *Nat. Nano* **2010**, *5*, 676.
(9) Gu, H.; Chao, J.; Xiao, S.-J.; Seeman, N. C. *Nature* **2010**, *465*, 202.
(10) Severcan, I.; Geary, C.; Chworos, A.; Voss, N.; Jacovetty, E.; Jaeger, L. *Nat. Chem.* **2010**, *2*, 772.
(11) Cutler, J. I.; Zhang, K.; Zheng, D.; Auyeung, E.; Prigodich, A. E.; Mirkin, C. A. *J. Am. Chem. Soc.* **2011**, *133*, 9254.
(12) Krishnan, Y.; Simmel, F. C. *Angew. Chem., Int. Ed.* **2011**, *50*, 3124.
(13) Macfarlane, R. J.; Lee, B.; Jones, M. R.; Harris, N.; Schatz, G. C.; Mirkin, C. A. *Science* **2011**, *334*, 204.
(14) Cutler, J. I.; Auyeung, E.; Mirkin, C. A. *J. Am. Chem. Soc.* **2012**, *134*, 1376.
(15) Fu, J.; Liu, M.; Liu, Y.; Yan, H. *Acc. Chem. Res.* **2012**, *45*, 1215.
(16) Wei, B.; Dai, M.; Yin, P. *Nature* **2012**, *485*, 623.
(17) Wilner, O. I.; Willner, I. *Chem. Rev.* **2012**, *112*, 2528.
(18) Li, Y.; Cu, Y. T. H.; Luo, D. *Nat. Biotechnol.* **2005**, *23*, 885.
(19) Lin, C.; Katilius, E.; Liu, Y.; Zhang, J.; Yan, H. *Angew. Chem., Int. Ed.* **2006**, *45*, 5296.
(20) Lin, C.; Liu, Y.; Yan, H. *Nano Lett.* **2007**, *7*, 507.
(21) Ke, Y.; Lindsay, S.; Chang, Y.; Liu, Y.; Yan, H. *Science* **2008**, *319*, 180.
(22) Pei, H.; Lu, N.; Wen, Y.; Song, S.; Liu, Y.; Yan, H.; Fan, C. *Adv. Mater.* **2010**, *22*, 4754.
(23) Pei, H.; Liang, L.; Yao, G.; Li, J.; Huang, Q.; Fan, C. *Angew. Chem., Int. Ed.* **2012**, *51*, 9020.
(24) Lee, J. B.; Roh, Y. H.; Um, S. H.; Funabashi, H.; Cheng, W.; Cha, J. J.; Kiatwuthinon, P.; Muller, D. A.; Luo, D. *Nat Nano* **2009**, *4*, 430.
(25) Chhabra, R.; Sharma, J.; Liu, Y.; Rinker, S.; Yan, H. *Adv. Drug Delivery Rev.* **2010**, *62*, 617.
(26) Hong, C. A.; Lee, S. H.; Kim, J. S.; Park, J. W.; Bae, K. H.; Mok, H.; Park, T. G.; Lee, H. *J. Am. Chem. Soc.* **2011**, *133*, 13914.
(27) Roh, Y. H.; Ruiz, R. C. H.; Peng, S.; Lee, J. B.; Luo, D. *Chem. Soc. Rev.* **2011**, *40*, 5730.
(28) Woo, S.; Rothemund, P. W. K. *Nat. Chem.* **2011**, *3*, 620.
(29) Hamblin, G. D.; Carneiro, K. M. M.; Fakhoury, J. F.; Bujold, K. E.; Sleiman, H. F. *J. Am. Chem. Soc.* **2012**, *134*, 2888.
(30) Crawford, R.; Erben, C. M.; Periz, J.; Hall, L. M.; Brown, T.; Turberfield, A. J.; Kapanidis, A. N. *Angew. Chem., Int. Ed.* **2013**, *52*, 2284.
(31) Zhu, G.; Zheng, J.; Song, E.; Donovan, M.; Zhang, K.; Liu, C.; Tan, W. *Proc. Natl. Acad. Sci. U.S.A.* **2013**, *110*, 7998.
(32) Grabow, W. W.; Jaeger, L. *Nat. Mater.* **2012**, *11*, 268.
(33) Lee, J. B.; Hong, J.; Bonner, D. K.; Poon, Z.; Hammond, P. T. *Nat. Mater.* **2012**, *11*, 316.
(34) Li, J.; Pei, H.; Zhu, B.; Liang, L.; Wei, M.; He, Y.; Chen, N.; Li, D.; Huang, Q.; Fan, C. *ACS Nano* **2011**, *5*, 8783.
(35) Lee, H.; Lytton-Jean, A. K. R.; Chen, Y.; Love, K. T.; Park, A. I.; Karagiannis, E. D.; Sehgal, A.; Querbes, W.; Zurenko, C. S.; Jayaraman, M.; Peng, C. G.; Charisse, K.; Borodovsky, A.; Manoharan, M.; Donahoe, J. S.; Truelove, J.; Nahrendorf, M.; Langer, R.; Anderson, D. G. *Nat Nano* **2012**, *7*, 389.
(36) Jiang, Q.; Song, C.; Nangreave, J.; Liu, X.; Lin, L.; Qiu, D.; Wang, Z.-G.; Zou, G.; Liang, X.; Yan, H.; Ding, B. *J. Am. Chem. Soc.* **2012**, *134*, 13396.
(37) Hughes, G. A. *J. Nanomed. Nanotechnol.* **2005**, *1*, 22.
(38) Lo, P. K.; Metera, K. L.; Sleiman, H. F. *Curr. Opin. Chem. Biol.* **2010**, *14*, 597.
(39) Kole, R.; Krainer, A. R.; Altman, S. *Nat. Rev. Drug Discovery* **2012**, *11*, 125.
(40) Nussbaumer, S.; Bonnabry, P.; Veuthey, J.-L.; Fleury-Souverain, S. *Talanta* **2011**, *85*, 2265.
(41) Zhu, G.; Meng, L.; Ye, M.; Yang, L.; Sefah, K.; O'Donoghue, M. B.; Chen, Y.; Xiong, X.; Huang, J.; Song, E.; Tan, W. *Chem.—Asian J.* **2012**, *7*, 1630.
(42) Shangguan, D.; Li, Y.; Tang, Z.; Cao, Z. C.; Chen, H. W.; Mallikaratchy, P.; Sefah, K.; Yang, C. J.; Tan, W. *Proc. Natl. Acad. Sci. U.S.A.* **2006**, *103*, 11838.
(43) Zhu, Z.; Wu, C.; Liu, H.; Zou, Y.; Zhang, X.; Kang, H.; Yang, C. J.; Tan, W. *Angew. Chem., Int. Ed.* **2010**, *49*, 1052.
(44) Yang, L.; Meng, L.; Zhang, X.; Chen, Y.; Zhu, G.; Liu, H.; Xiong, X.; Sefah, K.; Tan, W. *J. Am. Chem. Soc.* **2011**, *133*, 13380.
(45) Sefah, K.; Tang, Z. W.; Shangguan, D. H.; Chen, H.; Lopez-Colon, D.; Li, Y.; Parekh, P.; Martin, J.; Meng, L.; Phillips, J. A.; Kim, Y. M.; Tan, W. H. *Leukemia* **2009**, *23*, 235.
(46) Yang, J.; Chen, H.; Vlahov, I. R.; Cheng, J.-X.; Low, P. S. *Proc. Natl. Acad. Sci. U.S.A.* **2006**, *103*, 13872.

(47) Motomura, S.; Motoji, T.; Takanashi, M.; Wang, Y.-H.; Shiozaki, H.; Sugawara, I.; Aikawa, E.; Tomida, A.; Tsuruo, T.; Kanda, N.; Mizoguchi, H. *Blood* **1998**, *91*, 3163.
(48) Kesharwani, P.; Gajbhiye, V.; Jain, N. K. *Biomaterials* **2012**, *33*, 7138.
(49) Szakacs, G.; Paterson, J. K.; Ludwig, J. A.; Booth-Genthe, C.; Gottesman, M. M. *Nat. Rev. Drug Discovery* **2006**, *5*, 219.
(50) Meng, H.; Mai, W. X.; Zhang, H.; Xue, M.; Xia, T.; Lin, S.; Wang, X.; Zhao, Y.; Ji, Z.; Zink, J. I.; Nel, A. E. *ACS Nano* **2013**, *7*, 994.